bioRxiv preprint doi: https://doi.org/10.1101/2025.02.27.640173; this version posted March 3, 2025. The copyright holder for this preprint (which was not certified by peer review) is the author/funder, who has granted bioRxiv a license to display the preprint in perpetuity. It is made available under aCC-BY-NC-ND 4.0 International license.

Distinct chromatin regulators downmodulate meiotic axis formation and DNA break induction at chromosome ends

Adhithi R. Raghavan[1], Kieron May[2], Vijayalakshmi V. Subramanian[1,3], Hannah G. Blitzblau[1], Neem J. Patel[1], Jonathan Houseley[2], Andreas Hochwagen[1*]

Affiliations:

1. Department of Biology, New York University, New York, USA
2. Epigenetics Programme, Babraham Institute, Cambridge, UK
3. Department of Biology, IISER Tirupati, Tirupati, India

*Corresponding Author (andi@nyu.edu)

Current Affiliations: N.J.P. - Basecamp Research, London, UK

bioRxiv preprint doi: https://doi.org/10.1101/2025.02.27.640173; this version posted March 3, 2025. The copyright holder for this preprint (which was not certified by peer review) is the author/funder, who has granted bioRxiv a license to display the preprint in perpetuity. It is made available under aCC-BY-NC-ND 4.0 International license.

Abstract:

In many organisms, meiotic crossover recombination is suppressed near the extreme ends of chromosomes. Here, we identified two chromatin modifiers, the histone methyltransferase Dot1 and the Sir silencing complex, as regulators of this process in *Saccharomyces cerevisiae*. We show that the recombination-promoting axis proteins Red1 and Hop1, but not the axis-associated cohesin Rec8, are significantly reduced within 20 kb of telomeres compared to the chromosome interior. Dot1, which preferentially methylates histones in the chromosome interior, is required for this pattern by directing Red1 binding toward the chromosome interior. In parallel, the Sir complex suppresses the induction of meiotic DNA double-strand breaks (DSBs) at chromosome ends. Sir-dependent DSB suppression is independent of axis deposition and occurs in a chromosome end-specific manner that mirrors the spreading and transcriptional silencing activity of the complex, suggesting that the Sir complex suppresses DSB formation by limiting the openness of promoters, the preferred sites of meiotic DSB formation. We conclude that multiple chromatin-based mechanisms collaborate to achieve a robust reduction of meiotic recombination near chromosome ends.

Keywords: meiotic DSBs, subtelomeres, axis proteins, chromatin modifiers, Dot1, Sir2, Sir3

bioRxiv preprint doi: https://doi.org/10.1101/2025.02.27.640173; this version posted March 3, 2025. The copyright holder for this preprint (which was not certified by peer review) is the author/funder, who has granted bioRxiv a license to display the preprint in perpetuity. It is made available under aCC-BY-NC-ND 4.0 International license.

Introduction:

Meiosis is a specialized type of cell division that generates haploid gametes from diploid progenitor cells and plays an essential role in promoting genetic diversity[1]. Meiosis initiates with a single round of DNA replication followed by two rounds of chromosome segregation: the first segregates homologous chromosomes, and the second segregates sister chromatids[2,3]. Accurate segregation during meiosis I relies on meiotic crossover recombination, which exchanges DNA between homologous chromosome pairs and, together with sister chromatid cohesion, forms a physical connection between them[4]. Meiotic recombination is initiated by programmed double-strand breaks (DSBs), which are catalyzed by Spo11, a highly conserved topoisomerase-like enzyme[5].

Although DSBs can occur throughout the genome, their frequency varies widely. Chromosomal regions classified as “hot” experience frequent DSBs, whereas “cold” regions rarely undergo breakage[6]. This spatial regulation results from a complex interplay of factors, including local base composition, DNA accessibility, chromatin modifications, and meiotic chromosome architecture[5,7,8]. Meiosis-specific axis proteins, which localize at the base of the loop-axis structure of meiotic chromosomes, are also linked to DSB activity and the subsequent homolog-directed repair[6,9-11]. In *S. cerevisiae*, the axis proteins Red1 and Hop1 are required for both processes[11-14], and elevated levels of Red1 and Hop1 correlate with increased DSB formation and markers of crossover repair[15,16]. Red1 and Hop1 are recruited to the base of chromatin loops by the meiotic Rec8 cohesin complex but can also bind directly to chromatin through the nucleosome-binding activity of Hop1[14,15,17], leading to two independent modes of axis-dependent patterning of meiotic recombination.

In budding yeast, DSB activity is notably reduced within ~20 kb from telomeres[18]. This depletion is likely important for two reasons. First, the ends of chromosomes are enriched for repetitive DNA

bioRxiv preprint doi: https://doi.org/10.1101/2025.02.27.640173; this version posted March 3, 2025. The copyright holder for this preprint (which was not certified by peer review) is the author/funder, who has granted bioRxiv a license to display the preprint in perpetuity. It is made available under aCC-BY-NC-ND 4.0 International license.

sequences that are vulnerable to non-allelic homologous recombination (NAHR) and genome rearrangements[19]. Second, crossovers near chromosome ends are less effective at forming stable connections between homologous chromosomes and may lead to chromosome mis-segregation if they are the sole link between homolog pairs[20]. Indeed, recombination events near telomeres are linked to a higher risk of Trisomy 21 (Down syndrome) in humans[21,22].

S. cerevisiae chromosome ends consist of several distinct regions (**Fig. 1a**)[23,24]. In addition to telomerase-templated telomeric repeats that cap chromosome ends, “telomere-associated sequences” contain repetitive Y’ and X elements, while the “subtelomeric domains” extend inward for an average of about 20 kb from telomeres. Subtelomeric domains are relatively gene-poor regions enriched in gene families[25,26]. The telomeric repeats and X elements recruit the Sir2/Sir3/Sir4 histone deacetylase complex, establishing transcriptional silencing. This silent chromatin can spread over limited distances into the subtelomeric domains[27]. The subtelomeric domains, in turn, are defined by a unique chromatin signature, which includes a relative depletion of active chromatin marks[25,28].

Previous studies of meiotic recombination in *S. cerevisiae* have consistently shown a depletion of DSBs in X and Y’ elements as well as in subtelomeric domains[10,18,29]. While the mechanisms governing DSB suppression in X and Y’ elements remain largely unexplored, the reduced DSB levels in subtelomeric domains are accompanied by lower recruitment of DSB-promoting factors, such as Rec114[30], and diminished abundance of the axis protein Hop1[31]. Hop1, which recruits Rec114[11], is currently the most upstream regulator of recombination known to be depleted about 20 kb from the chromosome ends. However, the specific mechanisms controlling this altered distribution of Hop1—and whether its depletion is the sole driver of suppressed recombination near telomeres—are not understood.

Results:

bioRxiv preprint doi: https://doi.org/10.1101/2025.02.27.640173; this version posted March 3, 2025. The copyright holder for this preprint (which was not certified by peer review) is the author/funder, who has granted bioRxiv a license to display the preprint in perpetuity. It is made available under aCC-BY-NC-ND 4.0 International license.

The meiotic axis extends into the telomere-associated X and Y' sequences

Given the reduced axis protein enrichment near chromosome ends and their critical role in meiotic DSB formation and repair, we investigated how axis proteins interact with telomere-associated sequences and subtelomeric domains. These regions are often excluded from sequence-based analyses due to variations in telomere organization even among closely related yeast strains[24,32,33], and because the abundance of repetitive sequences and gene families creates challenges for uniquely assigning sequencing reads. Therefore, we tailored our analysis pipeline to account for these unique biological features. To reduce structural mapping artifacts, we mapped reads to high-quality end-to-end chromosome scaffolds of our experimental strain (SK1)[32], rather than the commonly used S288c reference. Further, by exclusively considering optimal matches, we maximized the number of confidently mapped reads, leveraging inherent sequence polymorphisms within telomeric repeat sequences for unique mapping. This approach resulted in high mapping success across all telomere-proximal regions **(Supplementary Fig. 1a)**. Even in the highly repetitive X and Y' elements, our pipeline uniquely mapped 12.81% and 0.87% of single-end reads and 15.18% and 12.80% of paired-end reads, respectively. In the subtelomeric domains, unique mapping rates were higher, averaging 24.07% for single-end reads and 32.21% for paired-end reads.

If a read had multiple equally good mapping results, our pipeline randomly selected one location as the primary alignment for the read. This approach did not affect metagene analyses but significantly improved signal clarity at individual chromosome ends by closing coverage gaps caused by a lack of polymorphisms. Comparative analysis of profiles with and without multiple mapping reads revealed no qualitative differences **(Supplementary Fig. 1b)**, supporting the robustness of our approach.

bioRxiv preprint doi: https://doi.org/10.1101/2025.02.27.640173; this version posted March 3, 2025. The copyright holder for this preprint (which was not certified by peer review) is the author/funder, who has granted bioRxiv a license to display the preprint in perpetuity. It is made available under aCC-BY-NC-ND 4.0 International license.

With this strategy, we analyzed the distribution of axis proteins at chromosome ends using previously published ChIP-seq datasets[14,31,34]. Meta-analysis revealed that Red1 and Hop1 were significantly less enriched than the genome average within 20 kb of chromosome ends **(Fig. 1b-c)**, consistent with previous studies[31]. Axis protein depletion was observed across all chromosome ends, and thus could not be attributed to individual telomere outliers **(Supplementary Fig. 2)**.

Yeast chromosome ends are characterized by telomeric repeats, $(TG_{1-3})_n$, and telomere-associated sequences, which include the Y’ and X elements[35]. The long Y’ elements (4-7 kb) are not found on all ends and can occur as one or multiple copies, whereas a short X element (~500 bp) is present at essentially all chromosome ends[32,36] **(Fig. 1a)**. Based on these features, we classified chromosome ends into two categories: X-only ends, which contain only the X element, and XY’ ends, which include both X and Y’ elements. Meta-plots of Red1 and Hop1 profiles revealed that axis protein enrichment differed between these two categories. X elements at X-only ends exhibited axis protein enrichment close to the genome average, indicating that isolated X elements have a substantial propensity for axis protein recruitment **(Fig. 1d)**. By contrast, X elements at XY’ ends showed Red1 and Hop1 enrichment below the genome average **(Fig. 1d),** suggesting that the presence of Y’ elements reduces axis protein binding on adjacent X elements **(Fig. 1f)**. This reduction may result from axis protein repositioning, as meta-analyses revealed an axis protein binding site at the telomere-proximal side of the Y’ element **(Fig. 1e).**

Multiple *cis*-acting features contribute to axis protein depletion near telomeres

Altered axis protein binding on adjacent X elements suggests that Y’ sequences may partially drive the telomere-proximal depletion of axis proteins observed in our meta-analysis **(Fig. 1b-c)**. In support of this, although both XY’ and X-only chromosome ends show reduced axis protein binding compared to the genome average, the depletion is stronger at XY’ ends **(Fig. 2a)**. These results indicate that Y’ elements contribute to the overall reduction of axis proteins at chromosome

bioRxiv preprint doi: https://doi.org/10.1101/2025.02.27.640173; this version posted March 3, 2025. The copyright holder for this preprint (which was not certified by peer review) is the author/funder, who has granted bioRxiv a license to display the preprint in perpetuity. It is made available under aCC-BY-NC-ND 4.0 International license.

ends. However, the observation that axis protein levels are also lower at X-only ends implies that additional mechanisms further suppress axis protein recruitment near telomeres.

To determine whether this additional mechanism is due to telomere proximity or intrinsic sequence features, we analyzed chromosome fusions, in which subtelomeric domains were relocated to the chromosome interior[37]. We observed that axis protein distribution at fused chromosome ends mirrored that of native, unfused ends **(Fig. 2b)**, suggesting that reduced axis protein enrichment at chromosome ends is driven by specific sequences encoded at chromosome ends rather than by telomere proximity.

Across the genome, gene-rich regions exhibit an overall higher axis protein enrichment[14,15]. As the subtelomeric domains are comparatively gene-poor[25,26], we plotted coding density (the fraction of DNA encoding open reading frames) as a function of distance from the telomeres. This analysis revealed a strong correlation between the regions of reduced coding density and axis protein depletion **(Fig. 2c)**, suggesting that reduced coding density may partially underlie the reduced axis protein recruitment within 20 kb of telomeres.

Rec8-dependent and independent pathways mediate axis protein localization at chromosome ends

Chromosomal recruitment of Red1 and Hop1 is mediated by two parallel pathways. The meiotic Rec8-cohesin complex preferentially recruits axis proteins to sites of convergent transcription[14], whereas the chromatin binding region (CBR) of Hop1 directs axis proteins to nucleosome-dense regions—“islands” characterized by higher coding density[15,17]. We sought to determine whether the depletion of axis proteins near chromosome ends could be attributed to the inactivity of one of these pathways.

bioRxiv preprint doi: https://doi.org/10.1101/2025.02.27.640173; this version posted March 3, 2025. The copyright holder for this preprint (which was not certified by peer review) is the author/funder, who has granted bioRxiv a license to display the preprint in perpetuity. It is made available under aCC-BY-NC-ND 4.0 International license.

Analysis of ChIP-seq data revealed that Rec8 is abundantly present at chromosome ends. Unlike Red1 and Hop1, Rec8-cohesin levels in the subtelomeric regions were comparable to the genome average **(Fig. 1b, c)**. Moreover, the regions enriched for Red1 and Hop1 in the telomere-associated sequences were also enriched for Rec8: Rec8 was bound more strongly to the X elements of X-only ends than to XY' ends **(Fig. 1d, f)** and formed a strong peak at the telomere-proximal side of Y' elements **(Fig. 1e)**. This peak coincided with the 3' end of the Y'-encoded open reading frame (ORF), consistent with other chromosomal Rec8 peaks, which are typically enriched downstream of ORFs[14,38]. Previous studies have demonstrated that active transcription can induce the sliding of the cohesin ring and direct axis protein association to the end of ORFs[14,39,40]. Therefore, transcription of the Y' ORF may similarly influence axis protein deposition within Y' elements.

The coincident binding of axis proteins and Rec8 supports the hypothesis that Rec8-cohesin is an important contributor to axis protein deposition at chromosome ends. To directly test this possibility, we examined Red1 binding in a *rec8* mutant strain using spike-in normalized ChIP-seq datasets[15,34]. In the subtelomeric domains, Red1 levels were significantly reduced in the *rec8* mutant compared to wild-type (**Fig. 3a-b**). However, Red1 binding was still detectable above baseline levels. Axis protein binding in the absence of Rec8 depends on the CBR domain of Hop1[15,17]. Indeed, the persistent subtelomeric axis protein signal in *rec8* mutants was abolished upon introduction of a Hop1 mutant (*hop1-phd*) lacking the CBR[15,17] **(Fig. 3a-b)**. By contrast, the *hop1-phd* mutation alone had comparatively minor effects in the subtelomeric domains, although we consistently noted reduced Red1 binding in the neighboring end-adjacent regions (EARs, 20-120 kb)[31] **(Fig. 3a-b)**. These data indicate that both pathways of axis recruitment additively contribute to Red1 binding at chromosome ends, with Rec8-cohesin responsible for recruiting the majority of Red1, consistent with the low coding density in these regions **(Fig. 2c)**. Similar additive

bioRxiv preprint doi: https://doi.org/10.1101/2025.02.27.640173; this version posted March 3, 2025. The copyright holder for this preprint (which was not certified by peer review) is the author/funder, who has granted bioRxiv a license to display the preprint in perpetuity. It is made available under aCC-BY-NC-ND 4.0 International license.

effects were observed in the X and Y' sequences **(Fig. 3c, d)**. Therefore, the selective inactivation of one recruitment pathway cannot explain the depletion of axis proteins in subtelomeric domains.

The methyltransferase Dot1 is required for subtelomeric depletion of axis proteins

Subtelomeric regions share qualitative similarities with pericentromeric regions, particularly in the differential enrichment of axis proteins and Rec8-cohesin. Both regions show a relatively higher abundance of Rec8-cohesin compared to Red1, with most data points falling below the genome-wide regression line **(Fig. 4a).** At pericentromeres, this differential enrichment of axis factors persists even if the centromere itself is inactivated[37], indicating that local DNA or chromatin environment influences axis protein binding. Given the distinct chromatin state of subtelomeric domains, we investigated whether chromatin modifiers specific to these regions contribute to axis protein depletion.

We focused our analysis on histone marks related to meiotic DSB formation[41,42] or those specifically different in the subtelomeric domains[28,42-44]. ChIP-seq analysis identified two marks - H3K4me3 and H3K79me3 - that closely matched the pattern of axis protein depletion **(Fig. 4b)**. Both marks are long-lasting indicators of active gene expression that are depleted from subtelomeric domains in vegetative cells [25,28] and have been implicated in the control of meiotic DSB formation[41,45]. To explore the role of these histone modifications in axis protein depletion, we used spike-in normalized ChIP-seq to analyze Red1 in mutants lacking Set1 or Dot1, the enzymes responsible for the trimethylation of H3K4 and H3K79, respectively[34]. In *set1Δ* mutants, subtelomeric Red1 binding patterns were indistinguishable from wild-type **(Fig. 4c-e)**. In contrast, Red1 levels in *dot1Δ* mutants were markedly elevated and no longer significantly different from the genome average **(Fig. 4c-e)**, suggesting that Dot1 suppresses axis protein binding in subtelomeric domains. Red1 levels were also elevated across Y' elements and moderately over X elements **(Fig. 4g, h)**. Notably, pericentromeric axis protein recruitment in *dot1Δ* mutants did

bioRxiv preprint doi: https://doi.org/10.1101/2025.02.27.640173; this version posted March 3, 2025. The copyright holder for this preprint (which was not certified by peer review) is the author/funder, who has granted bioRxiv a license to display the preprint in perpetuity. It is made available under aCC-BY-NC-ND 4.0 International license.

not show a statistically significant difference by bootstrapping analysis, although the average binding values were slightly reduced compared to wild-type **(Fig. 4f)**. In contrast, subtelomeric regions exhibited the opposite effect, with average binding levels increasing in *dot1Δ* mutants **(Fig. 4e)**.

Subtelomeric regions in wild-type cells are undermethylated on H3K79 **(Fig. 4b)**, suggesting that the role of Dot1 in axis protein regulation may be indirect. In line with this interpretation, spike-in normalized ChIP-seq data showed that the increased Red1 binding in subtelomeric regions of *dot1Δ* mutants was accompanied by lower Red1 levels in the chromosome interior **(Fig. 4c-e)**. To probe which axis recruitment pathway is regulated by Dot1, we separated Red1 signals into genic and intergenic regions, as Hop1 primarily recruits Red1 to gene bodies, whereas Rec8-cohesin leads to Red1 enrichment in intergenic regions[14]. The reduced binding of Red1 in the chromosome interior in *dot1Δ* mutants primarily affected intergenic regions, implying that Dot1 promotes Rec8-dependent axis binding. Consistent with this interpretation, the increase in Red1 association near chromosome ends in *dot1Δ* mutants occurred predominantly on gene bodies **(Fig. 4i)**. These data indicate that the chromatin requirements for axis recruitment differ between chromosome ends and the chromosome interior, and that Dot1 helps direct Red1 to chromosome interiors by promoting Rec8-dependent axis recruitment.

Conservation of Sir-dependent telomeric heterochromatin during meiotic recombination

One consequence of *DOT1* disruption is the spreading of the Sir complex beyond its usual boundaries[46,47]. Indeed, the mislocalization of Sir2 and Sir3 in *dot1* mutants was previously linked to checkpoint defects during meiotic recombination[48]. To investigate this link further, we examined the role of the Sir complex in suppressing axis protein deposition and DSB formation at chromosome ends.

bioRxiv preprint doi: https://doi.org/10.1101/2025.02.27.640173; this version posted March 3, 2025. The copyright holder for this preprint (which was not certified by peer review) is the author/funder, who has granted bioRxiv a license to display the preprint in perpetuity. It is made available under aCC-BY-NC-ND 4.0 International license.

In vegetative cells, the Sir complex establishes silent chromatin domains at mating-type loci and telomere-associated sequences[49,50]. At some chromosome ends, Sir chromatin also spreads from the X element into the neighboring subtelomeric domains[27,51], although spreading across entire subtelomeric domains is only observed under conditions of Sir overexpression[28]. We used ChIP-seq analysis to assess Sir3's chromatin association and spreading during meiotic prophase.

Our observations at the time of meiotic induction and during the peak of DSB formation (3 hours post-induction) revealed consistent binding patterns **(Fig. 5a)**. Although Sir3 was enriched at both types of X elements, its binding on X elements at XY' ends was lower than that observed at X-only ends **(Fig. 5a, c)**. Sir3 was also enriched upstream of the Y'-encoded ORF, but binding was relatively diminished across the Y' ORF **(Fig. 5b)**. Additionally, we observed heterogeneous spreading of Sir3 from subtelomeric X elements into adjacent subtelomeric domains on certain chromosome ends. For example, on chrVII-L, Sir3 spread approximately 6 kb from the X element during early prophase I (3 hours post-meiotic induction) **(Fig. 5d)**, while there was no apparent spreading on chrVI-L **(Fig. 5e)**. The extent of Sir3 spreading varied substantially and did not correlate with the presence of Y' elements but mirrored the distribution of Sir proteins in vegetative cells[27,28]. These findings indicate that Sir-dependent telomeric heterochromatin remains largely unchanged as cells initiate meiotic recombination.

Sir3 spreading into subtelomeric domains suppresses meiotic transcription but does not affect axis protein deposition.

To determine whether subtelomeric domains with Sir3 spreading exhibit altered transcription of underlying genes, we conducted mRNA-seq analysis on samples collected 3 hours post-meiotic induction in the presence or absence of *SIR3*. Plotting relative fold changes in mRNA levels as a function of the average Sir3 occupancy in the associated promoter region (250bp upstream of each gene), revealed a significant correlation between Sir3 occupancy and increased mRNA

bioRxiv preprint doi: https://doi.org/10.1101/2025.02.27.640173; this version posted March 3, 2025. The copyright holder for this preprint (which was not certified by peer review) is the author/funder, who has granted bioRxiv a license to display the preprint in perpetuity. It is made available under aCC-BY-NC-ND 4.0 International license.

levels upon *SIR3* deletion **(Fig. 6a**) in the 5 kb regions adjacent to the X element where Sir3 frequently spreads. These results indicate that the transcriptional effects of Sir3 are confined to sequences where Sir3 spreading occurs, as detected by ChIP-seq.

Given the prominent Sir3 peak observed at the start of the Y' element metaplot **(Fig. 5b)**, we also analyzed Y' element expression at 3 hours post-meiotic induction. The average Y' element expression was significantly increased in the absence of *SIR3* (**Supplementary Fig. 3**). These results suggest that the absence of *SIR3* impacts Y' element transcription.

We asked whether deletion of *SIR3* also affects the deposition of axis proteins near chromosome ends by determining the distribution of Red1 in *sir3* mutants using spike-in normalized ChIP-seq analysis. Meta-analysis revealed no significant difference in the average depletion of Red1 in the last 20 kb between *sir3* and wild-type strains **(Supplementary Fig. 4a, b)**. Similarly, meta-plots of average Red1 profiles on X and Y' elements in *sir3* mutants showed no new peaks compared to wild-type **(Supplementary Fig. 4c, d)**, although enrichment levels were lower on both types of X element **(Supplementary Fig. 4c)**. The overall genome-wide median binding levels of Red1 were higher in the *sir3* mutants **(Supplementary Fig. 4b)**, aligning with the previously reported analyses of Hop1[31]. These findings indicate that Sir3 binding, and the establishment of silent chromatin domains do not result in large-scale alterations to the binding landscape of axis proteins at chromosome ends. They also imply that the altered axis protein binding seen in *dot1* mutants is not a consequence of the increased Sir complex spreading in this mutant.

Sir proteins protect X elements and regions of Sir spreading from meiotic DSBs

We wondered how Sir-dependent heterochromatin and Dot1-dependent axis protein suppression interface with the meiotic DSB machinery near chromosome ends. Genome-wide DSB levels had previously been determined in *sir2Δ* strains using Spo11-oligo sequencing, which sequences the DNA fragments that remain covalently attached to Spo11 after cleavage[31,52], but telomere-

bioRxiv preprint doi: https://doi.org/10.1101/2025.02.27.640173; this version posted March 3, 2025. The copyright holder for this preprint (which was not certified by peer review) is the author/funder, who has granted bioRxiv a license to display the preprint in perpetuity. It is made available under aCC-BY-NC-ND 4.0 International license.

proximal DSB formation had not been investigated in that study. Analysis of this dataset revealed a significant increase in DSB levels on X elements but not on Y’ elements in *sir2Δ* strains **(Fig. 6b**). This pattern mirrors the relative enrichment of Sir3 in these elements, indicating that Sir chromatin suppresses DSB formation in the X elements.

We also observed increased DSB formation in the subtelomeric domains in *sir2Δ* mutants. Increased DSB induction was correlated with the extent of Sir3 occupancy in wild-type cells **(Fig. 6c)**. Accordingly, increased DSB formation also correlated with elevated gene expression in the same regions in *sir3* mutants but not in the rest of the genome **(Fig. 6d)**. These findings suggest that elevated promoter openness, which enables increased gene expression, also creates a window for meiotic DSB formation.

To complement and expand this analysis, we analyzed *sir3* and *dot1Δ* mutants by TrAEL-seq, which sequences the exposed 3’ ends that result from Spo11 removal[53]. To avoid signal changes due to DSB repair, this analysis was conducted in a repair-defective *dmc1Δ* background[54]. TrAEL-seq analysis at the 5-hour time point showed a distinct increase in DSB formation within 20 kb of telomeres in *sir3* mutants, with the number of significant DSB hotspots nearly doubling within 5 kb of X elements **(Fig. 6e, f)**. On the other hand, DSB formation was unaffected in the same regions in *dot1Δ* mutants **(Fig. 6e, f)**. Accordingly, TrAEL-seq analysis of *sir3 dot1Δ* double mutants revealed DSB patterns similar to *sir3* single mutants **(Fig. 6e, f)**. Moreover, a substantial level of DSB suppression persisted even in the double mutant **(Fig. 6e, Supplementary Fig. 5b)**, indicating that additional layers of regulation contribute to DSB suppression at chromosome ends (see Discussion).

Intriguingly, TrAEL-seq analysis indicated differing genetic interactions between *DOT1* and *SIR3* in other parts of the genome. DSB levels dropped in the subtelomere-adjacent EARs, specifically in *dot1Δ sir3* double mutants, suggesting redundant functions **(Supplementary Fig. 5a)**, whereas

bioRxiv preprint doi: https://doi.org/10.1101/2025.02.27.640173; this version posted March 3, 2025. The copyright holder for this preprint (which was not certified by peer review) is the author/funder, who has granted bioRxiv a license to display the preprint in perpetuity. It is made available under aCC-BY-NC-ND 4.0 International license.

DSB formation around centromeres was decreased to a similar extent in *dot1Δ* and *sir3* single mutants **(Supplementary Fig. 5b)**. Finally, around the ribosomal DNA locus, DSB levels were increased in a Sir3-dependent manner in *dot1Δ* mutants **(Supplementary Fig. 5c)**, consistent with previously observed Sir-dependent DSB induction in this region[55]. These findings imply a combinatorial code that allows these two chromatin regulators to adjust meiotic recombination in a region-specific manner.

Discussion:

Here we show that meiotic recombination potential at chromosome ends is suppressed by at least two mechanisms. First, the local depletion of axis proteins, which regulate the recruitment of key DSB factors and help target DSBs toward recombination with the homologous chromosome. Second, telomeric heterochromatin restricts access to gene promoters, the preferred DNA substrates for DSB formation in yeast[10] **(Fig. 7)**. These mechanisms thus represent distinct strategies for regulating meiotic recombination potential.

The range of these two mechanisms differs significantly. Dot1-dependent axis protein depletion spans the entire subtelomeric domain and exhibits consistent patterns across chromosome ends, with variability largely driven by the distribution of axis binding sites[14]. In contrast, Sir-dependent DSB suppression is highly variable among chromosome ends, driven by the extent of Sir-dependent chromatin spreading. This variability in heterochromatin spread is also observed in vegetative cells, where boundaries are influenced by transcription factor binding sites, genic elements, and nucleosome-disfavoring DNA sequences [25,56-60].

While Sir-dependent chromatin spreading directly suppresses DSB hotspots, Dot1 likely influences axis deposition indirectly **(Fig. 7)**, as H3K79 trimethylation occurs predominantly in the chromosome interior[25]. Our findings demonstrate that the *dot1Δ* mutation causes a genome-wide redistribution of Red1, with reduced binding in the chromosomal interior. Because Red1 levels

bioRxiv preprint doi: https://doi.org/10.1101/2025.02.27.640173; this version posted March 3, 2025. The copyright holder for this preprint (which was not certified by peer review) is the author/funder, who has granted bioRxiv a license to display the preprint in perpetuity. It is made available under aCC-BY-NC-ND 4.0 International license.

are limiting[61], one potential explanation is that the absence of Dot1 releases Red1 from intergenic regions, enabling it to bind gene bodies in the subtelomeric domains **(Supplementary Fig. 6)**. Intriguingly, the *hop1-phd* mutant, which should also release some Red1 because of its failure to bind to gene bodies across the genome[15], does not exhibit similar increases in Red1 binding at subtelomeric domains **(Fig. 2a)**, raising the possibility that the increased axis recruitment to subtelomeric domains in *dot1Δ* mutants requires the CBR domain.

Although subtelomeric regions in *dot1Δ* mutants exhibit increased DSB potential due to Red1 redistribution, this does not result in substantial increases in DSB formation, even in *sir3 dot1Δ* double mutants in which the suppressive effect of the Sir complex is eliminated. We speculate that the absence of a stronger effect may be the consequence of increased DSB turnover, which would not be detected by our TrAEL-seq analyses. Dot1 is required for the meiotic arrest of *dmc1Δ* mutants[48]. As a result, repair foci disappear in *dot1Δ dmc1Δ* mutants as cells progress into meiosis I, with breaks repaired via Rad54-dependent inter-sister recombination[48]. Moreover, additional regulatory layers of telomere-proximal DSB suppression must exist because a significant level of DSB suppression persists even in *sir3 dot1Δ* double mutants. These layers may include further chromatin-based mechanisms. Additionally, one likely contributor is the low coding density of subtelomeric regions as the lower density of gene promoters inherently results in a smaller number of potential DSB hotspots. Indeed, the regional drop in coding density correlates well with reduced axis protein recruitment and DSB formation. Our analysis of axis deposition in chromosome fusion strains also supports this notion. Thus, to some extent the low DSB potential may be hardwired into the genome sequence of chromosome ends. The combined action of multiple pathways suppressing recombination at chromosome ends likely ensures that meiotic crossovers are strongly disfavored near telomeres. Telomere-proximal crossovers are less effective at maintaining linkages between homologous chromosomes[62] and are associated with increased risk of Down syndrome in humans[21,22,63,64]. The downmodulation of axis proteins

bioRxiv preprint doi: https://doi.org/10.1101/2025.02.27.640173; this version posted March 3, 2025. The copyright holder for this preprint (which was not certified by peer review) is the author/funder, who has granted bioRxiv a license to display the preprint in perpetuity. It is made available under aCC-BY-NC-ND 4.0 International license.

in subtelomeric regions may play a critical role in this process, as axis proteins not only recruit DSB factors but also help target DSB repair to homologous chromosomes by preventing sister chromatid recombination[65]. Although a low level of DSBs occurs in telomere-associated regions and subtelomeric domains[10], reduced axis protein abundance likely makes these regions less prone to crossover formation. Favoring repair from sister chromatids may also reduce the risk of non-allelic recombination events. Non-allelic recombination is especially risky at chromosome ends due to their repetitive sequences and the close physical proximity of telomeres along the nuclear envelope during meiotic prophase[19,66,67]. These multiple regulatory layers thus establish a robust protective mechanism to shield chromosome ends from non-allelic and unproductive recombination and ensure proper meiotic chromosome segregation.

Methods and Materials:

Yeast strains and growth conditions:

All the strains utilized in this study belonged to the SK1 background (except for the analysis using the published fusion chromosomes, which are SK1 and S288C hybrids). The genotypes are detailed in **Supplementary Table 1.** For experiments using vegetative cells, mid-logarithmic phase cultures were grown in YPD medium overnight at room temperature until saturation. On the following day, the cells were diluted to an OD600 of 0.2 and incubated at 30°C until they reached an OD600 of 1. At this stage, 50 ml of culture was collected for ChIP-seq.

To induce synchronous meiotic cultures, strains were grown for 24 hours in YPD medium at room temperature. Cells were enriched in the G1 phase by inoculating them at OD600 = 0.3 in pre-sporulation BYTA medium (1% yeast extract, 2% bactotryptone, 1% potassium acetate, 50 mM potassium phthalate) for 16.5 hours at 30°C. Cells were washed twice with sterile water and transferred into SPO medium at OD600 = 1.9 (SPO: 0.3% potassium acetate, 0.001% acetic acid). Cultures were grown at 30°C on a shaker, and the time of inoculation into SPO was defined

bioRxiv preprint doi: https://doi.org/10.1101/2025.02.27.640173; this version posted March 3, 2025. The copyright holder for this preprint (which was not certified by peer review) is the author/funder, who has granted bioRxiv a license to display the preprint in perpetuity. It is made available under aCC-BY-NC-ND 4.0 International license.

as time = 0. At specific timepoints, 25 ml of culture was collected for ChIP-seq and 1.6 ml for mRNA-seq. The synchrony of meiotic cultures was validated using Fluorescence-activated cell sorting (FACS).

FACS:

Cells collected at various timepoints were fixed overnight at 4°C in 350 µl of absolute ethanol. Cells were pelleted and incubated in 500 µl FACS buffer (50 mM sodium citrate) with 0.7 µl RNase A (20–40 mg/ml stock; Sigma-Aldrich) and 5 µl proteinase K (20 mg/ml; VWR) for 24 hours at 50°C. Prior to FACS analysis, cells were stained with 0.1 µl SYTOX Green (5 mM solution in DMSO; Invitrogen) and briefly sonicated for 5 seconds at 10% amplitude. DNA content was analyzed using the BD FACSAria II system at the Genomics Core at New York University Center for Genomics and Systems Biology.

Chromatin immunoprecipitation (ChIP) & Illumina sequencing:

The cells collected at the indicated timepoints were pelleted and immediately crosslinked for 30 minutes in a 1% formaldehyde solution at room temperature with gentle shaking. Subsequently, the crosslinking reaction was quenched by incubating the cells for 5 minutes at room temperature in a 125 mM glycine solution. Following this, the cells were processed according to the protocol outlined in[68] and immunoprecipitated with 2.5 µl of either anti-Sir3 (HM01065, a kind gift from the Bell lab) or anti-Red1 (#16440, kind gift of N. Hollingsworth) or anti-H3K79me3 (abcam, ab2621). Library preparation, quality, and quantity checks were then performed as described in [17]. All the prepared chromatin immunoprecipitation (ChIP) libraries were sequenced as 150-bp paired-end reads on Illumina NextSeq 500 instruments. The sequencing run was conducted by the Genomics Core at New York University Center for Genomics and Systems Biology.

Processing ChIP -seq reads from Illumina sequencing:

bioRxiv preprint doi: https://doi.org/10.1101/2025.02.27.640173; this version posted March 3, 2025. The copyright holder for this preprint (which was not certified by peer review) is the author/funder, who has granted bioRxiv a license to display the preprint in perpetuity. It is made available under aCC-BY-NC-ND 4.0 International license.

Illumina sequencing reads were aligned to the SK1 genome[32] using Bowtie 2 (Version 2.4.2)[69]. To improve mapping of reads to repetitive subtelomeric regions, the Bowtie 2 read reporting mode was configured to allow multiple alignments, reporting the best match[69]. MACS2 2.1.1 was used to extend reads in the 5'-> 3' direction to a final length of 200 bp. SPMR (signal per million reads) normalization was applied to both Input and ChIP pileups using MACS2. The resulting fold-enrichment files were used for downstream analysis in R. The ChIP-seq pipeline and analysis scripts are available on the Hochwagen Lab GitHub page https://github.com/hochwagenlab/ChromosomeEnds.git.

mRNA-sequencing & analysis:

mRNA extraction, first- and second-strand synthesis, and library preparation were conducted following the procedures outlined in[70]. The resulting libraries were subjected to sequencing as 150-bp paired-end reads on Illumina NextSeq 500 instruments. The sequencing run was executed by the Genomics Core at New York University Center for Genomics and Systems Biology. The GTF (General Transfer Format) file was modified to include all completely annotated Y’ elements. Subsequently, reads obtained from Illumina sequencing were aligned to the SK1 genome[32], and the counts mapping to the modified SK1 gtf file were determined using the nf-core RNA-Seq pipeline[71,72]. The relative abundances, measured as Transcripts per million (TPM) in the Salmon[73] output file "salmon.merged.gene_counts_length_scaled.rds", were utilized for downstream analysis in R.

Spo11-oligos mapping:

In this study, previously published Spo11-oligos datasets from WT and *sir2Δ* strains[31,52] were utilized. Adaptors were removed from the reads using fastx_clipper from the FASTX-Toolkit (version 0.0.14) and reads shorter than 15 bp were discarded. Subsequently, the clipped reads were aligned to the SK1 genome[32] using Bowtie 2 (Version 2.4.2)[69] . The read alignment mode

bioRxiv preprint doi: https://doi.org/10.1101/2025.02.27.640173; this version posted March 3, 2025. The copyright holder for this preprint (which was not certified by peer review) is the author/funder, who has granted bioRxiv a license to display the preprint in perpetuity. It is made available under aCC-BY-NC-ND 4.0 International license.

was set to local, and the reporting mode allowed multiple read alignments while reporting the best alignment[69]. Following alignment, MACS2 2.2 (https://github.com/taoliu/MACS) was employed to extend reads in the 5'→3' direction to a final length of 37 bp[74]. SPMR (signal per million reads) normalization was performed on the pileups.

Plug preparation for TrAEL-seq:

Plugs were prepared from meiotic cultures harvested 5 hours into meiosis. For each strain, 20 ml of culture was pelleted and washed twice with CHEF TE buffer (10 mM Tris-HCl, pH 7.5, 50 mM EDTA, pH 8.0). The cell pellet was resuspended in 300 µl CHEF TE, followed by the addition of 4 µl zymolyase (10 mg/ml). The mixture was briefly vortexed and incubated at 42°C for approximately 30 seconds. Low-melting-point agarose (1% SeaPlaque GTG in 125 mM EDTA, pH 8.0), prewarmed to 42°C, was added and transferred into plug molds. Plugs were solidified on ice for 10 minutes before being transferred into LET buffer (10 mM Tris-HCl, pH 7.5; 0.5 M EDTA, pH 8.0). Plugs were incubated overnight at 37°C.

The following day, plugs were treated with proteinase K in NDS buffer (10 mM Tris-HCl, pH 7.5; 0.5 M EDTA; 1% N-lauroylsarcosine) at 50°C overnight. After digestion, plugs were washed sequentially: first with CHEF TE for 1 hour at room temperature, followed by two washes with CHEF TE containing 10 µl freshly prepared PMSF (100 mM) in ethanol, with each wash incubated for 1 hour in the cold room. A fourth wash was performed with RNase T1 in CHEF TE, incubated at 37°C for 1 hour, followed by a final wash with CHEF TE at room temperature for 1 hour. Plugs were stored at 4°C in CHEF TE until further use.

TrAEL-seq Library Preparation, Sequencing, and Data Analysis:

TrAEL-seq library preparation, sequencing and data analysis were conducted following the procedures outlined in [53]. TrAEL-seq signal pileups were generated using MACS2 (v2.2) and

bioRxiv preprint doi: https://doi.org/10.1101/2025.02.27.640173; this version posted March 3, 2025. The copyright holder for this preprint (which was not certified by peer review) is the author/funder, who has granted bioRxiv a license to display the preprint in perpetuity. It is made available under aCC-BY-NC-ND 4.0 International license.

normalized pileups were generated using SPMR normalization. Downstream analyses were done in R.

Supporting information: Supplementary Figures and Tables are attached in a word document.

Data reporting: The datasets generated and analyzed in this paper, excluding published datasets, have been deposited in the Gene Expression Omnibus (GEO). The datasets can be accessed with the accession number for ChIP-seq: GSExxxxxx, for RNA-seq: GSExxxxxx, and for TrAEL-seq: GSExxxxxx. Additionally, all ChIP-seq datasets used in this study are described in **Supplementary Table 2**, and all Spo11-oligos, RNA-seq and TrAEL-seq datasets are described in **Supplementary Table 3**.

Conflict of interest: The authors declare no conflicting interests.

Acknowledgements:

We express our sincere gratitude to Stephen P. Bell for generously providing the Sir3 antibody and to Nancy Hollingsworth for the Red1 antibody. We also acknowledge the Genomics Core at the New York University Center for Genomics and Systems Biology for their valuable technical assistance and expertise in data processing. This work was supported in part by the NYU IT High-Performance Computing resources, services, and staff expertise. We are grateful to the Zegar Family Foundation for their generous support. TrAEL-seq library sequencing and processing were performed by the Genomics (Geno06) and Bioinformatics (Bioinf01) teams at the Babraham Institute, which receive financial support from the Institute Core Capability Grant (BBSRC CCG). This research was financially supported as part of NIH grant R35 GM148223 to AH. ARR acknowledges support from a Fleur Strand Graduate Fellowship from the Department of Biology, as well as a Henry MacCracken Fellowship and a Dean’s Dissertation Fellowship from the NYU Graduate School of Arts and Science. JH acknowledges funding from the BBSRC (BI Epigenetics

bioRxiv preprint doi: https://doi.org/10.1101/2025.02.27.640173; this version posted March 3, 2025. The copyright holder for this preprint (which was not certified by peer review) is the author/funder, who has granted bioRxiv a license to display the preprint in perpetuity. It is made available under aCC-BY-NC-ND 4.0 International license.

ISP; BBS/E/B/000C0523), and KM acknowledges funding from the BBSRC (BB/W509917/1). The funders had no role in the preparation of this manuscript.

Author contributions: Conceptualization - A.R.R., V.V.S., H.G.B., and A.H; Investigation & Formal analysis - A.R.R., K.M., V.V.S., H.G.B., N.J.P., J.H., A.H; Computational Pipeline development - A.R.R.; Manuscript writing (initial draft) - A.R.R. and A.H.; Manuscript editing - all authors.

Figures:

bioRxiv preprint doi: https://doi.org/10.1101/2025.02.27.640173; this version posted March 3, 2025. The copyright holder for this preprint (which was not certified by peer review) is the author/funder, who has granted bioRxiv a license to display the preprint in perpetuity. It is made available under aCC-BY-NC-ND 4.0 International license.

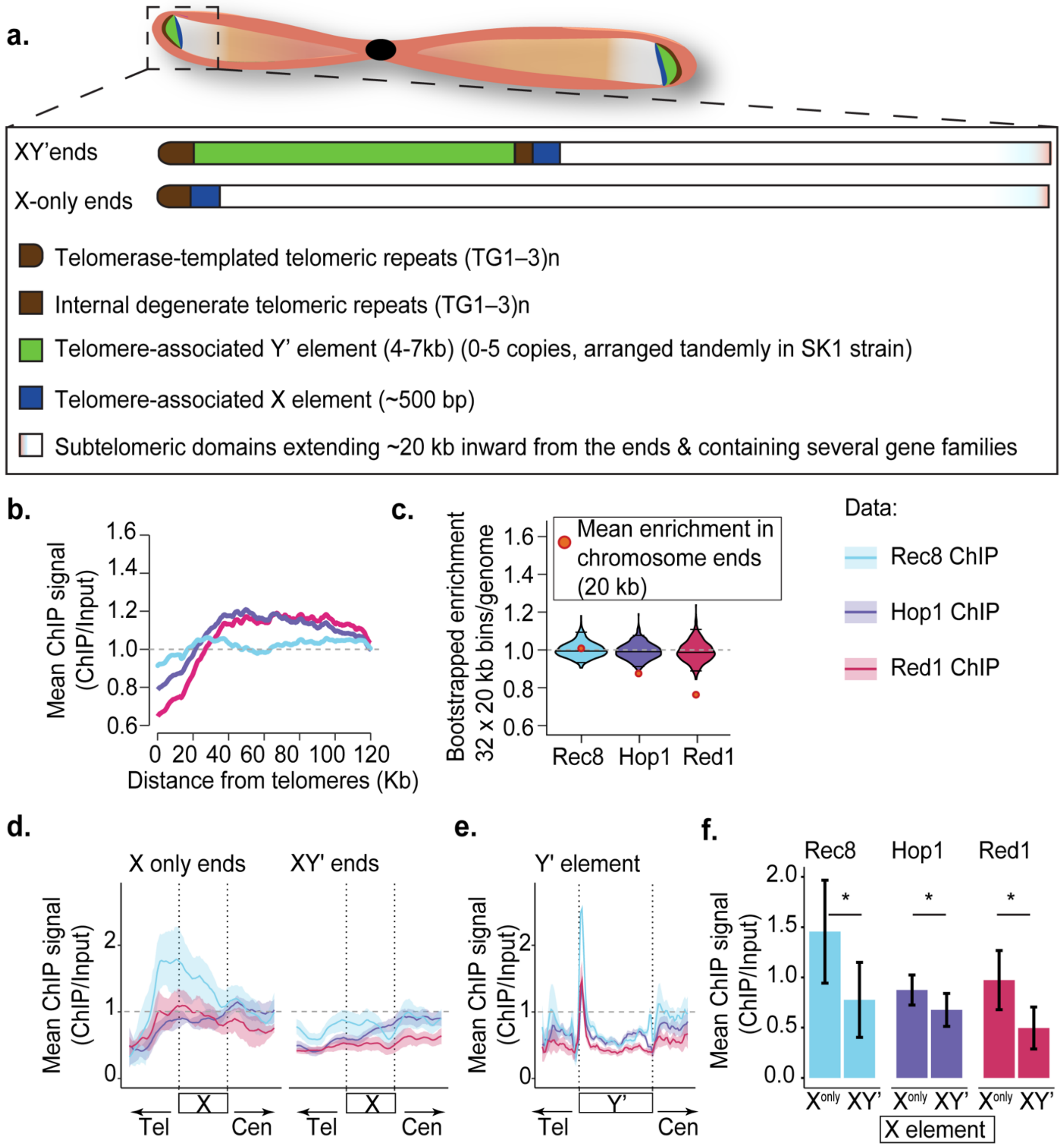

Raghavan *et al*, Fig. 1

Fig. 1: Meiotic axis extends to the telomere-associated sequences. (a) Schematic representation of the distinct regions present at chromosome ends in *Saccharomyces cerevisiae*. Black dot represents the centromere. **(b)** Mean fold enrichment of Rec8, Red1, and Hop1 relative to their distance from telomeres, using published ChIP-seq datasets from WT cells at early

bioRxiv preprint doi: https://doi.org/10.1101/2025.02.27.640173; this version posted March 3, 2025. The copyright holder for this preprint (which was not certified by peer review) is the author/funder, who has granted bioRxiv a license to display the preprint in perpetuity. It is made available under aCC-BY-NC-ND 4.0 International license.

prophase I (3 hours)[14]. **(c)** Bootstrapped distributions of fold enrichment within thirty-two 20 kb bins spanning the genome. Median values and two-sided 95% confidence intervals are shown as black horizontal lines, with orange/red circles highlighting the mean enrichment in the last 20 kb of chromosome ends. **(d, e)** Meta-plots of average Rec8, Red1, and Hop1 enrichment at chromosome end-associated X and Y' elements. Vertical dotted lines mark the positions of the X or Y' element. For X elements, regions of equal size adjacent to the X element on both the centromere-proximal (Cen) and telomere-proximal (Tel) sides are shown. For Y' elements, adjacent regions equal to half the size of the Y' element are shown. Genome averages are denoted by gray horizontal dashed lines, and colored solid lines with shaded areas represent the mean and two-sided 95% confidence intervals for each protein. **(f)** Bar plots comparing Rec8, Hop1, and Red1 levels on X elements in X-only and XY' ends. Normality of the data was assessed using the Shapiro-Wilk test. Significance was determined using Student's two-sided t-test (*$p \leq 0.05$) (raw p-values: 0.0186, 0.0058, 0.0079), with Benjamini-Hochberg p-value adjustment (BH corrected p-values: 0.0186, 0.0118, 0.0118). Effect sizes were estimated using Cohen's d: Rec8 (d = 1.62), Hop1 (d = 1.13), and Red1 (d = 0.89). All the data presented here are averages of two independent biological replicates, and the results were reproducible between replicates.

bioRxiv preprint doi: https://doi.org/10.1101/2025.02.27.640173; this version posted March 3, 2025. The copyright holder for this preprint (which was not certified by peer review) is the author/funder, who has granted bioRxiv a license to display the preprint in perpetuity. It is made available under aCC-BY-NC-ND 4.0 International license.

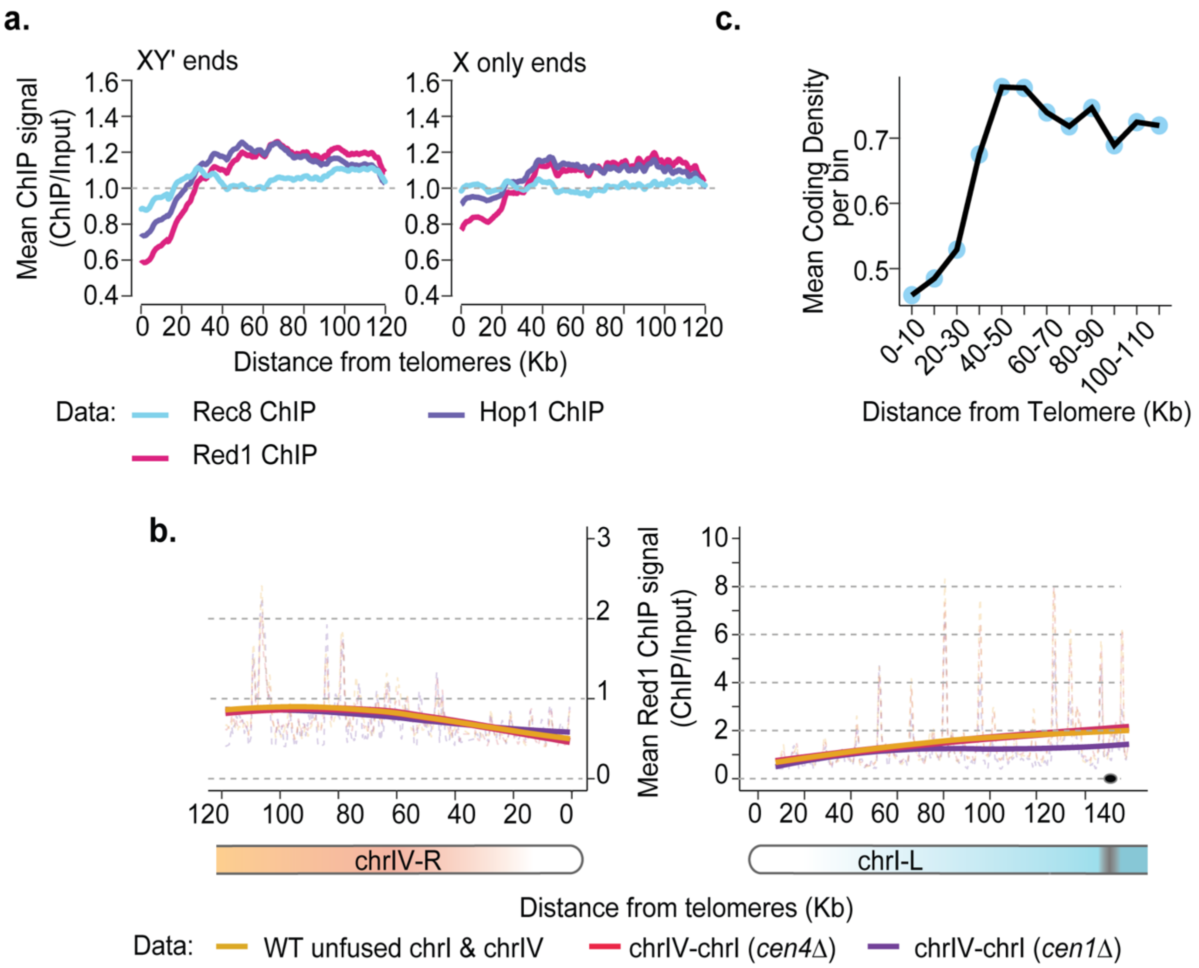

Raghavan *et al*, Fig. 2

Fig. 2: Multiple *cis*-acting features contribute to axis protein depletion near telomeres. (a) Meta-plots of Rec8, Hop1, and Red1 ChIP enrichment (ChIP/Input) at XY' and X-only chromosome ends, aligned by their distance from telomeres. The genome-wide average enrichment is indicated by a dashed gray line. Data are derived from published ChIP-seq datasets of WT cells at early prophase I (3 hours)[14,31,34]. **(b)** Analysis of Red1 binding in SK1/S288C hybrids containing unfused (WT) or homozygous fusion (chrIV-chrI) chromosomes, using published datasets[37]. Dashed lines represent signal traces, and solid-colored lines represent loess-normalized regressions. The black dot marks the position of *CEN1*. **(c)** Coding density as a function of distance from telomeres, averaged across chromosome ends per bin. Blue dots

bioRxiv preprint doi: https://doi.org/10.1101/2025.02.27.640173; this version posted March 3, 2025. The copyright holder for this preprint (which was not certified by peer review) is the author/funder, who has granted bioRxiv a license to display the preprint in perpetuity. It is made available under aCC-BY-NC-ND 4.0 International license.

indicate mean coding density per bin, and the black line connects these means. Coding density is calculated as the fraction of DNA encoding open reading frames. All the data presented here are averages of two independent biological replicates, and the results were reproducible between replicates.

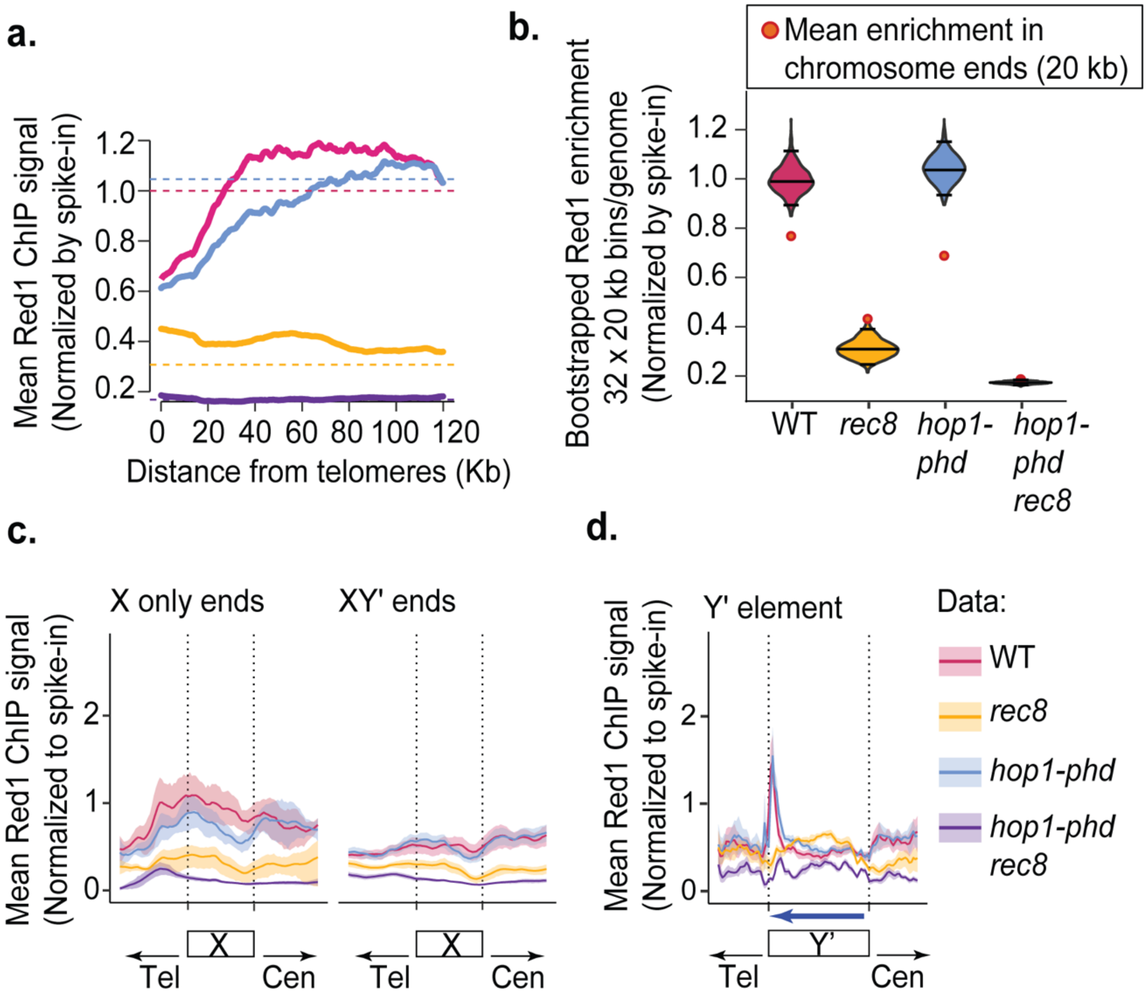

Fig. 3: Differential recruitment of Red1 at chromosome ends by Rec8-dependent and independent pathways. (a) Meta-plots of average Red1 enrichment (spike-in normalized) at various distances from telomeres in WT, *rec8*, *hop1-phd*, *and hop1-phd rec8* strains during early prophase I (3 hours). Data are derived from spike-in normalized SNP ChIP-seq datasets[15]. The

bioRxiv preprint doi: https://doi.org/10.1101/2025.02.27.640173; this version posted March 3, 2025. The copyright holder for this preprint (which was not certified by peer review) is the author/funder, who has granted bioRxiv a license to display the preprint in perpetuity. It is made available under aCC-BY-NC-ND 4.0 International license.

colored dashed lines represent the genome average for each strain after spike-in normalization. **(b)** Bootstrapped distributions of Red1 enrichment within thirty-two 20 kb bins across the genome, with medians and two-sided 95% confidence intervals indicated by black lines. Mean enrichment in the last 20 kb of chromosome ends is highlighted with orange/red circles. **(c, d)** Meta-plots of average Red1 enrichment on X and Y’ elements at chromosome ends. Vertical dotted lines mark the positions of X and Y’ elements. Adjacent regions—of the same size for X elements or half-sized for Y’ elements—are included both telomere (Tel) and centromere (Cen) proximal to the elements. Colored solid lines represent mean enrichment, with shaded areas depicting two-sided 95% confidence intervals for each strain. The blue arrow denotes the transcription direction of the Y’ ORF. All the data presented here are averages of two independent biological replicates, and the results were reproducible between replicates.

bioRxiv preprint doi: https://doi.org/10.1101/2025.02.27.640173; this version posted March 3, 2025. The copyright holder for this preprint (which was not certified by peer review) is the author/funder, who has granted bioRxiv a license to display the preprint in perpetuity. It is made available under aCC-BY-NC-ND 4.0 International license.

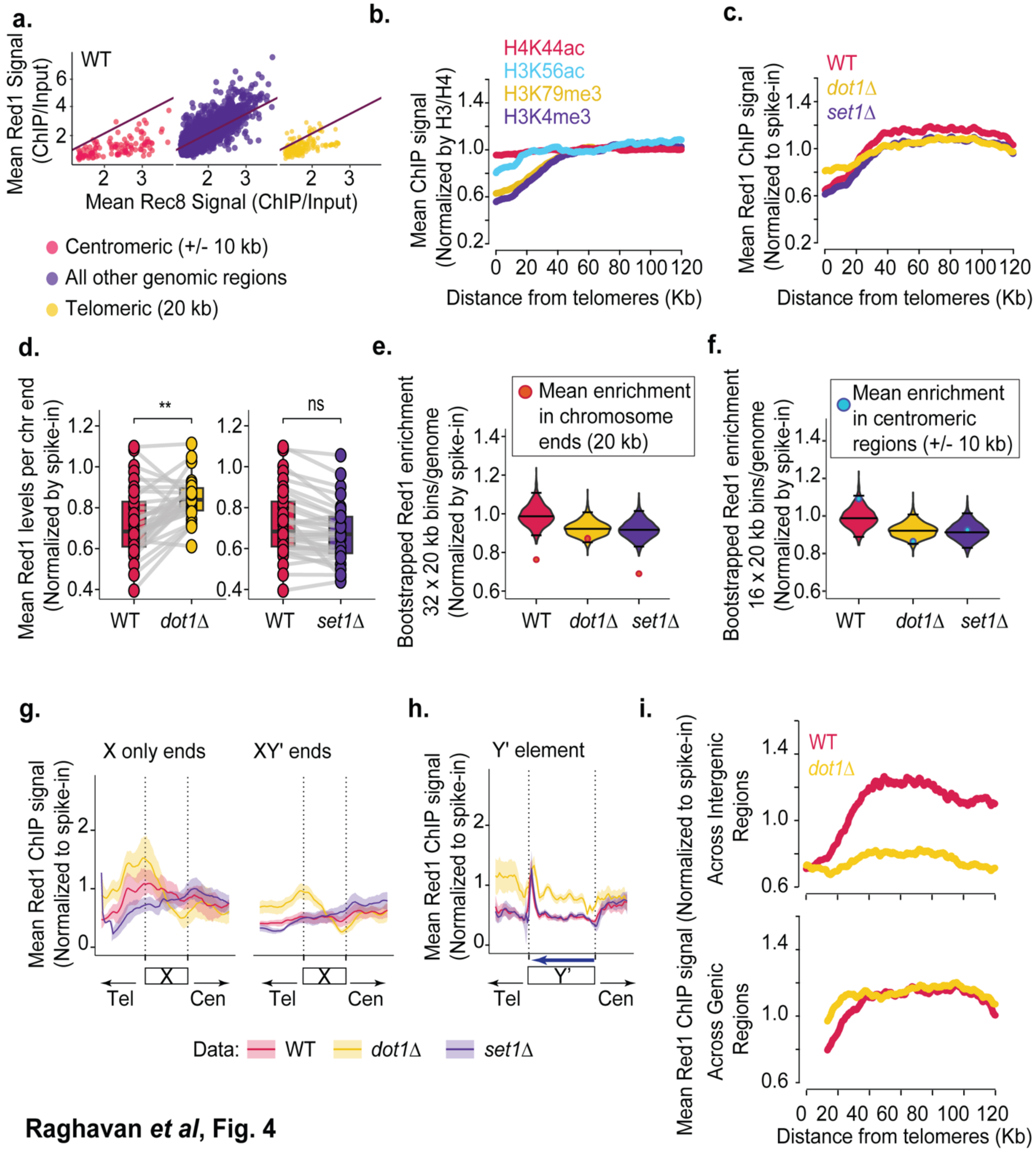

Raghavan *et al*, Fig. 4

Fig. 4: Dot1 regulates axis protein distribution at chromosome ends and interior regions. **(a)** Scatter plot comparing Red1 and Rec8 levels at individual Rec8 peaks across three genomic regions: pericentromeric regions (±10 kb from centromeres), non-pericentromeric/non-telomeric regions, and chromosome ends (last 20 kb). Genome-wide trend lines illustrate the overall

bioRxiv preprint doi: https://doi.org/10.1101/2025.02.27.640173; this version posted March 3, 2025. The copyright holder for this preprint (which was not certified by peer review) is the author/funder, who has granted bioRxiv a license to display the preprint in perpetuity. It is made available under aCC-BY-NC-ND 4.0 International license.

correlation between Red1 and Rec8 (slope of linear regression trendline = 1.34). Data are derived from published WT ChIP-seq datasets[14]. **(b)** Mean histone acetylation and methylation marks (H4K44ac, H3K56ac, H3K4me3, and H3K79me3), normalized to H4 or H3, plotted as a function of distance from chromosome ends using published datasets as well as experimental datasets[42,44]. **(c)** Spike-in normalized Red1 levels in WT, *dot1Δ*, and *set1Δ* mutants, plotted as a function of distance from chromosome ends using published datasets[34]. **(d)** Boxplots of mean Red1 levels per chromosome end (20 kb) in WT, *dot1Δ*, and *set1Δ* mutants. Circles represent mean signals for individual chromosome ends, with lines connecting matched chromosome ends across strains. Normality of the data was assessed using the Shapiro-Wilk test. Student's two-sided t-test $^{**}p \leq 0.01$, ns – non significant (raw p-values: 0.001891863, 0.181274230), Benjamini-Hochberg p-value adjusted (BH corrected p-values: 0.003783726, 0.181274230). Effect sizes were estimated using Cohen's d: WT vs. *dot1Δ* (d = -0.82); WT vs. *set1Δ* (d = 0.34). **(e, f)** Bootstrapped distributions of Red1 enrichment within (e) thirty-two 20 kb bins and (f) sixteen 20 kb bins, spanning the genome. Median values and two-sided 95% confidence intervals are shown as black horizontal lines. Orange/red circles in **(e)** indicate mean enrichment at the last 20 kb of chromosome ends, and blue circles in **(f)** highlight mean enrichment at ±10 kb around centromeres. **(g, h)** Meta-plots of Red1 enrichment on X and Y' elements. Vertical dotted lines indicate the positions of X and Y' elements. Adjacent regions, of the same size for X elements or half-sized for Y' elements, are shown telomere (Tel) and centromere (Cen) proximal. Colored solid lines represent mean enrichment, with shaded areas showing two-sided 95% confidence intervals for each strain. The blue arrow denotes the transcription direction of the Y' ORF. **(i)** Meta-analysis of Red1 distribution in WT and *dot1Δ* mutants, separated into intergenic (top panel) and genic regions (bottom panel), plotted as a function of distance from chromosome ends using spike-in normalized values. All the data presented here are averages of two independent biological replicates, and the results were reproducible between replicates.

bioRxiv preprint doi: https://doi.org/10.1101/2025.02.27.640173; this version posted March 3, 2025. The copyright holder for this preprint (which was not certified by peer review) is the author/funder, who has granted bioRxiv a license to display the preprint in perpetuity. It is made available under aCC-BY-NC-ND 4.0 International license.

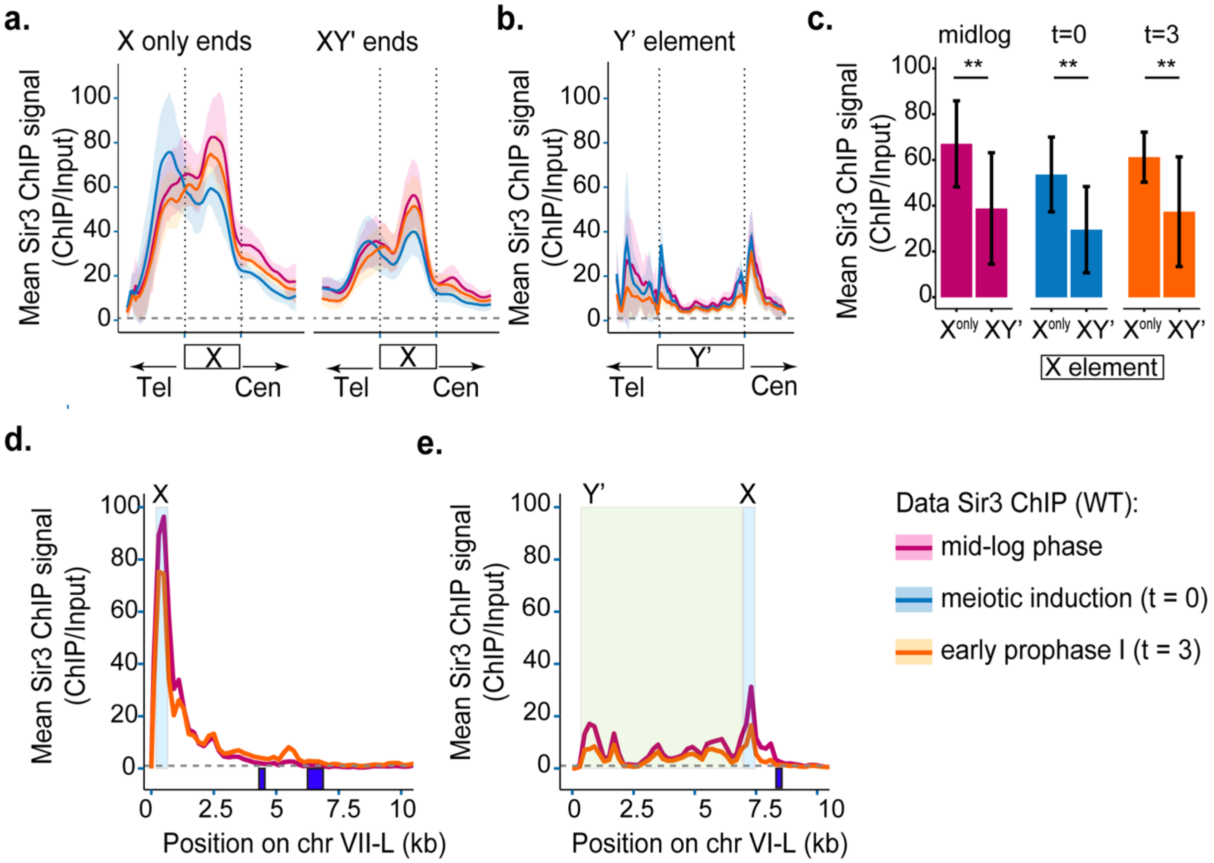

Raghavan *et al*, Figure 5

Fig. 5: Sir3 spreads heterogeneously from the X element during meiotic prophase I. (a, b) Meta-plots of Sir3 ChIP enrichment in wild-type (WT) strains at X elements and Y' elements during mid-log phase, meiotic induction (time = 0 hours), and early prophase I (time = 3 hours). Vertical dotted lines indicate the positions of X and Y' elements. Adjacent regions—of the same size for X elements or half-sized for Y' elements—are shown both telomere (Tel) and centromere (Cen) proximal. **(c)** Bar plots comparing Sir3 enrichment at X elements in X-only and XY' chromosome ends during mid-log phase, meiotic induction (time = 0 hours), and early prophase I (time = 3 hours). Normality of the data was assessed using the Shapiro-Wilk test. Student's two-sided t-test **p ≤ 0.01 (raw p-values: 0.007263657, 0.007243783, 0.001837521), Benjamini-Hochberg p-value adjusted (BH corrected p-values: 0.007263657, 0.007263657, 0.005512564). Effect sizes were estimated using Cohen's d: Sir3 mid-log phase (d = 1.22); meiotic induction (d = 1.32); early

bioRxiv preprint doi: https://doi.org/10.1101/2025.02.27.640173; this version posted March 3, 2025. The copyright holder for this preprint (which was not certified by peer review) is the author/funder, who has granted bioRxiv a license to display the preprint in perpetuity. It is made available under aCC-BY-NC-ND 4.0 International license.

prophase I (d = 1.11). **(d, e)** Sir3 binding profiles on chrVII-L **(d)** and chrVI-L **(e)** during mid-log phase and early meiotic prophase I (time = 3 hours). ChrVII-L shows detectable spreading of Sir3 from the X element into adjacent gene-poor regions, while no detectable spreading is observed on chrVI-L. ORFs are annotated in blue. All the data presented here are averages of two independent biological replicates, and the results were reproducible between replicates.

bioRxiv preprint doi: https://doi.org/10.1101/2025.02.27.640173; this version posted March 3, 2025. The copyright holder for this preprint (which was not certified by peer review) is the author/funder, who has granted bioRxiv a license to display the preprint in perpetuity. It is made available under aCC-BY-NC-ND 4.0 International license.

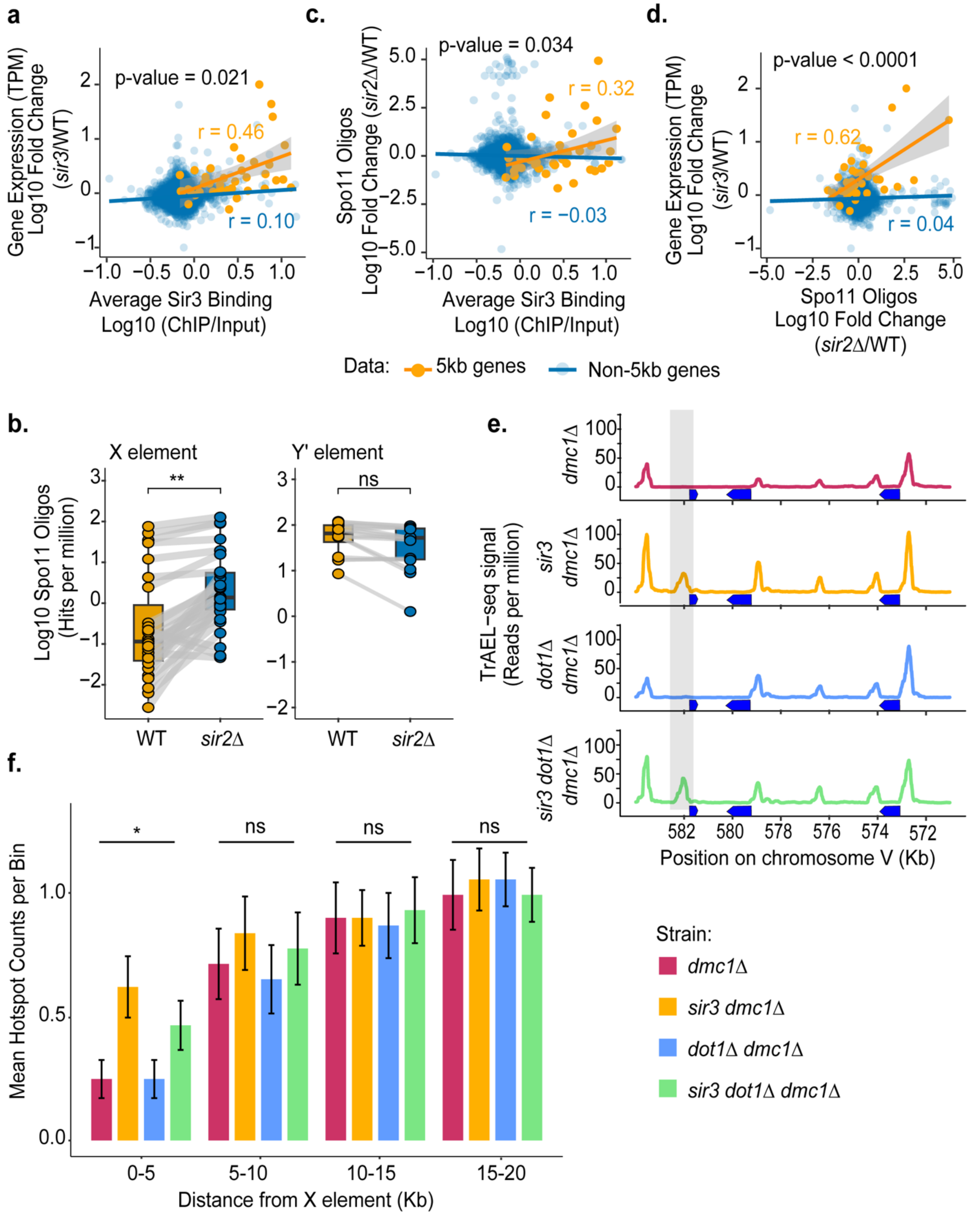

566 **Raghavan *et al*, Fig. 6**

bioRxiv preprint doi: https://doi.org/10.1101/2025.02.27.640173; this version posted March 3, 2025. The copyright holder for this preprint (which was not certified by peer review) is the author/funder, who has granted bioRxiv a license to display the preprint in perpetuity. It is made available under aCC-BY-NC-ND 4.0 International license.

Fig. 6: Sir proteins protect X elements and regions of spread from meiotic DSBs. (a) Scatter plot of gene expression fold change (*sir3*/WT, measured in *ndt80Δ* background) versus Sir3 binding (log10 ChIP/Input) in promoter regions for 5 kb genes (yellow) and non-5 kb genes (blue) at 3 hours post-meiotic induction. Pearson correlation coefficients (r) were calculated in R using the cor() function (Pearson method) and serve as the measure of effect size. p-values were computed using Fisher Z-transformation (two-sided test) to enable statistical testing of correlation significance. Outliers (top and bottom 1% quantiles for 5 kb genes and three non-5 kb gene outliers) were excluded. **(b)** Boxplots of log10-transformed Spo11-oligo signals (hits per million) at X and Y' elements in WT and s*ir2Δ* strains. Data are derived from published Spo11-oligo datasets[29,50]. Circles represent total scores for individual elements, with lines connecting matched elements across strains. Normality of the data was assessed using the Shapiro-Wilk test. Since the data did not meet normality assumptions, the Wilcoxon rank-sum test was used to compare groups. Wilcoxon rank-sum test (two-sided) $^{**}p \leq 0.01$; ns - not significant (raw p-values: 0.00179054, 0.15670080), with Benjamini-Hochberg p-value adjustment (BH adjusted p-values: 0.003581081, 0.156700804). Effect sizes were estimated using Rank-Biserial Correlation (RBC) (r = -0.707, -0.408). **(c)** Scatter plot of Spo11-oligo fold change (*sir2Δ*/WT) in promoter regions as a function of average Sir3 binding (log10 ChIP/Input) in the same promoter regions. Yellow points represent genes within 5 kb of X elements, and blue points represent non-5 kb genes. Pearson correlation coefficients (r) serve as the measure of effect size, and p-values were computed as in (a). Outliers (top and bottom 1% quantiles for 5 kb genes and three outliers from non-5 kb genes) were excluded. **(d)** Scatter plot of gene expression fold change (*sir3*/WT, measured in *ndt80Δ* strains) as a function of Spo11-oligo fold change (*sir2Δ*/WT) in promoter regions for genes within 5 kb of X elements (yellow) and non-5 kb genes (blue). Pearson correlation coefficients (r) serve as the measure of effect size, and p-values were computed as in (a). **(e)** TrAEL-seq signal tracks for chromosome V-R subtelomeric regions in the indicated strains. Blue boxes represent

bioRxiv preprint doi: https://doi.org/10.1101/2025.02.27.640173; this version posted March 3, 2025. The copyright holder for this preprint (which was not certified by peer review) is the author/funder, who has granted bioRxiv a license to display the preprint in perpetuity. It is made available under aCC-BY-NC-ND 4.0 International license.

annotated ORFs. The highlighted region (gray) marks a peak present in *sir3 dmc1Δ* and *sir3 dot1Δ dmc1Δ* but absent in *dmc1Δ* and *dot1Δ dmc1Δ*. **(f)** Mean hotspot counts per 5 kb bin as a function of distance from X elements for the indicated strains. Hotspots were identified using peaks called as significant from TrAEL-seq data. Error bars represent the standard error of the mean. Normality of the data was assessed using the Shapiro-Wilk test. Since the data did not meet normality assumptions, the Wilcoxon rank-sum test was used to compare groups. Statistical significance was assessed using a Kruskal-Wallis two-sided test to compare hotspot counts across bins. *p ≤ 0.05; ns - not significant (Raw p-values: 0.04066, 0.8046, 0.9805, 0.9118). All the data presented here are averages of two independent biological replicates, and the results were reproducible between replicates.

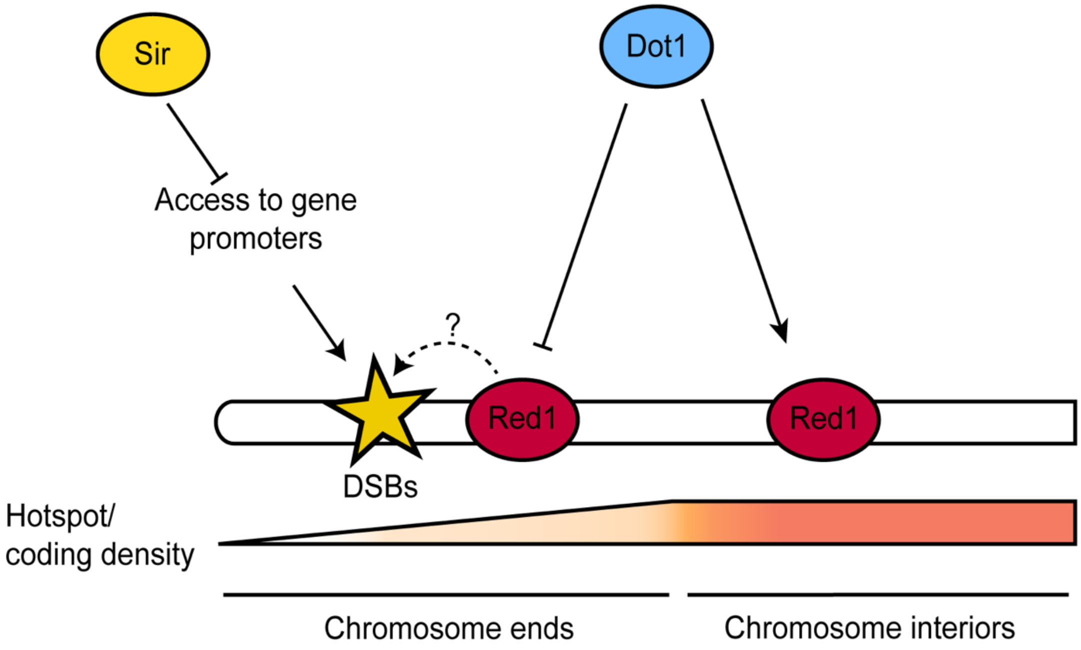

Raghavan *et al*, Fig. 7

bioRxiv preprint doi: https://doi.org/10.1101/2025.02.27.640173; this version posted March 3, 2025. The copyright holder for this preprint (which was not certified by peer review) is the author/funder, who has granted bioRxiv a license to display the preprint in perpetuity. It is made available under aCC-BY-NC-ND 4.0 International license.

Fig. 7: Model showing distinct mechanisms of DSB regulation at chromosome ends by Sir3 and Dot1. Sir proteins restrict promoter accessibility at chromosome ends, thereby influencing DSB formation in these regions. In contrast, Dot1 prevents Red1 accumulation at chromosome ends by directing it to chromosome interiors. Whether the decreased Red1 levels contribute to lower DSB levels or increased sister repair at chromosome ends similar to the rest of the genome remains unresolved (dashed line with a question mark). Orange shading represents coding/hotspot density.

bioRxiv preprint doi: https://doi.org/10.1101/2025.02.27.640173; this version posted March 3, 2025. The copyright holder for this preprint (which was not certified by peer review) is the author/funder, who has granted bioRxiv a license to display the preprint in perpetuity. It is made available under aCC-BY-NC-ND 4.0 International license.

References:

1. Mozzachiodi, S. & Liti, G. Evolution of yeast hybrids by aborted meiosis. *Current Opinion in Genetics and Development* **77**, 101980-101980 (2022).
2. Börner, G.V., Hochwagen, A. & MacQueen, A.J. Meiosis in budding yeast. *Genetics* **225**, 1-33 (2023).
3. Duro, E. & Marston, A.L. From equator to pole: Splitting chromosomes in mitosis and meiosis. *Genes and Development* **29**, 109-122 (2015).
4. Hunter, N. Meiotic recombination: The essence of heredity. *Cold Spring Harbor Perspectives in Biology* **7**(2015).
5. Arter, M. & Keeney, S. Divergence and conservation of the meiotic recombination machinery. *Nature Reviews Genetics* **25**, 309-325 (2024).
6. Lichten, M. Meiotic chromatin: The substrate for recombination initiation. *Genome Dynamics and Stability* **3**, 165-193 (2008).
7. Raghavan, A.R. & Hochwagen, A. Keeping it safe: control of meiotic chromosome breakage. *Trends in Genetics* (2024).
8. Ito, M. & Shinohara, A. Chromosome architecture and homologous recombination in meiosis. *Front Cell Dev Biol* **10**, 1097446 (2022).
9. Mohibullah, N. & Keeney, S. Numerical and spatial patterning of yeast meiotic DNA breaks by Tel1. *Genome Research* **27**(2017).
10. Pan, J. *et al.* A hierarchical combination of factors shapes the genome-wide topography of yeast meiotic recombination initiation. *Cell* **144**, 719-731 (2011).
11. Panizza, S. *et al.* Spo11-accessory proteins link double-strand break sites to the chromosome axis in early meiotic recombination. *Cell* **146**, 372-383 (2011).
12. Schwacha, A. & Kleckner, N. Interhomolog Bias during Meiotic Recombination: Meiotic Functions Promote a Highly Differentiated Interhomolog-Only Pathway. in *Cell* Vol. 90 1123-1135 (Keeney and Kleckner, 1997).
13. Hollingsworth, P.L. Making it Through Parenting. *Gifted Child Today Magazine* **13**, 2-7 (1990).
14. Sun, X. *et al.* Transcription dynamically patterns the meiotic chromosome-axis interface. *eLife* **4**, 1-23 (2015).
15. Heldrich, J. *et al.* Two pathways drive meiotic chromosome axis assembly in *Saccharomyces cerevisiae*. *Nucleic Acids Research* **50**, 4545-4556 (2022).
16. Joshi, N., Barot, A., Jamison, C. & Börner, G.V. Pch2 links chromosome axis remodeling at future crossover sites and crossover distribution during yeast meiosis. *PLoS Genet* **5**, e1000557 (2009).
17. Milano, C.R. *et al.* Chromatin binding by HORMAD proteins regulates meiotic recombination initiation. *EMBO Journal* **43**, 836-867 (2024).
18. Blitzblau, H.G., Bell, G.W., Rodriguez, J., Bell, S.P. & Hochwagen, A. Mapping of Meiotic Single-Stranded DNA Reveals Double-Strand-Break Hotspots near Centromeres and Telomeres. *Current Biology* **17**, 2003-2012 (2007).
19. Sasaki, M., Lange, J. & Keeney, S. Genome destabilization by homologous recombination in the germ line. *Nature Reviews Molecular Cell Biology* **11**, 182-195 (2010).

bioRxiv preprint doi: https://doi.org/10.1101/2025.02.27.640173; this version posted March 3, 2025. The copyright holder for this preprint (which was not certified by peer review) is the author/funder, who has granted bioRxiv a license to display the preprint in perpetuity. It is made available under aCC-BY-NC-ND 4.0 International license.

20. Ross, L.O., Maxfield, R. & Dawson, D. Exchanges are not equally able to enhance meiotic chromosome segregation in yeast. *Proceedings of the National Academy of Sciences of the United States of America* **93**(1996).

21. Oliver, T.R. *et al.* New insights into human nondisjunction of chromosome 21 in oocytes. *PLoS Genet* **4**, e1000033 (2008).

22. Ghosh, S., Feingold, E. & Dey, S.K. Etiology of Down syndrome: Evidence for consistent association among altered meiotic recombination, nondisjunction, and maternal age across populations. *Am J Med Genet A* **149a**, 1415-20 (2009).

23. Pryde, F.E., Gorham, H.C. & Louis, E.J. Chromosome ends: all the same under their caps. *Curr Opin Genet Dev* **7**, 822-8 (1997).

24. Louis, E.J. The chromosome ends of *Saccharomyces cerevisiae*. *Yeast* **11**, 1553-1573 (1995).

25. Hocher, A. & Taddei, A. Subtelomeres as Specialized Chromatin Domains. *BioEssays* **42**(2020).

26. Fabre, E. & Spichal, M. Subnuclear Architecture of Telomeres and Subtelomeres in Yeast. in *Subtelomeres* (eds. Louis, E.J. & Becker, M.M.) 13-37 (Springer Berlin Heidelberg, Berlin, Heidelberg, 2014).

27. Brothers, M. & Rine, J. Distinguishing between recruitment and spread of silent chromatin structures in *Saccharomyces cerevisiae*. *eLife* **11**, 1-23 (2022).

28. Hocher, A. *et al.* Expanding heterochromatin reveals discrete subtelomeric domains delimited by chromatin landscape transitions. *Genome Research* **28**, 1852-1866 (2018).

29. Buhler, C., Borde, V. & Lichten, M. Mapping meiotic single-strand DNA reveals a new landscape of DNA double-strand breaks in *Saccharomyces cerevisiae*. *PLoS Biology* **5**, 2797-2808 (2007).

30. Murakami, H. *et al.* Multilayered mechanisms ensure that short chromosomes recombine in meiosis. *Nature* (2020).

31. Subramanian, V.V. *et al.* Persistent DNA-break potential near telomeres increases initiation of meiotic recombination on short chromosomes. *Nature Communications* **10**, 1-15 (2019).

32. Yue, J.X. *et al.* Contrasting evolutionary genome dynamics between domesticated and wild yeasts. *Nature Genetics* **49**, 913-924 (2017).

33. D'Angiolo, M. *et al.* Telomeres are shorter in wild *Saccharomyces cerevisiae* isolates than in domesticated ones. *Genetics* **223**(2023).

34. Vale-Silva, L.A., Markowitz, T.E. & Hochwagen, A. SNP-ChIP: A versatile and tag-free method to quantify changes in protein binding across the genome. *BMC Genomics* **20**, 1-10 (2019).

35. Kwapisz, M. & Morillon, A. Subtelomeric Transcription and its Regulation. *Journal of molecular biology* **432**, 4199-4219 (2020).

36. Wellinger, R.J. & Zakian, V.A. Everything you ever wanted to know about S*accharomyces cerevisiae* telomeres: Beginning to end. *Genetics* **191**, 1073-1105 (2012).

37. Luo, J. *et al.* Synthetic chromosome fusion: Effects on mitotic and meiotic genome structure and function. *Cell Genomics* **3**(2023).

38. Glynn, E.F. *et al.* Genome-wide mapping of the cohesin complex in the yeast *Saccharomyces cerevisiae. PLoS Biology* **2**(2004).

bioRxiv preprint doi: https://doi.org/10.1101/2025.02.27.640173; this version posted March 3, 2025. The copyright holder for this preprint (which was not certified by peer review) is the author/funder, who has granted bioRxiv a license to display the preprint in perpetuity. It is made available under aCC-BY-NC-ND 4.0 International license.

39. Ocampo-Hafalla, M.T. & Uhlmann, F. Cohesin loading and sliding. *Journal of Cell Science* **124**, 685-691 (2011).
40. Bausch, C. *et al.* Transcription Alters Chromosomal Locations of Cohesin in *Saccharomyces cerevisiae*. *Molecular and Cellular Biology* **27**, 8522-8532 (2007).
41. Borde, V. *et al.* Histone H3 lysine 4 trimethylation marks meiotic recombination initiation sites. *EMBO Journal* **28**, 99-111 (2009).
42. Hu, J. *et al.* H4K44 Acetylation Facilitates Chromatin Accessibility during Meiosis. *Cell Reports* **13**, 1772-1780 (2015).
43. Gothwal, S.K. *et al.* The double-strand break landscape of meiotic chromosomes is shaped by the Paf1 transcription elongation complex in *Saccharomyces cerevisiae*. *Genetics* **202**, 497-512 (2016).
44. Zhu, X. & Keeney, S. High-resolution global analysis of the influences of Bas1 and Ino4 transcription factors on meiotic DNA break distributions in *saccharomyces cerevisiae*. *Genetics* **201**, 525-542 (2015).
45. Bani Ismail, M., Shinohara, M. & Shinohara, A. Dot1-dependent histone H3K79 methylation promotes the formation of meiotic double-strand breaks in the absence of histone H3K4 methylation in budding yeast. *PLoS ONE* **9**(2014).
46. Takahashi, Y.-H. *et al.* Dot1 and Histone H3K79 Methylation in Natural Telomeric and HM Silencing. *Molecular Cell* **42**, 118-126 (2011).
47. Shilatifard, A. Chromatin modifications by methylation and ubiquitination: Implications in the regulation of gene expression. *Annual Review of Biochemistry* **75**, 243-269 (2006).
48. San-Segundo, P.A. & Roeder, G.S. Role for the Silencing Protein Dot1 in Meiotic Checkpoint Control. in *Molecular Biology of the Cell* Vol. 11 3601-3615 (2000).
49. Hoppe, G.J. *et al.* Steps in Assembly of Silent Chromatin in Yeast: Sir3-Independent Binding of a Sir2/Sir4 Complex to Silencers and Role for Sir2-Dependent Deacetylation. *Molecular and Cellular Biology* **22**, 4167-4180 (2002).
50. Rusche, L.N., Kirchmaier, A.L. & Rine, J. The Establishment, Inheritance, and Function of Silenced Chromatin in *Saccharomyces cerevisiae*. *Annual Review of Biochemistry* **72**, 481-516 (2003).
51. Pryde, F.E. & Louis, E.J. Limitations of silencing at native yeast telomeres. *EMBO Journal* **18**, 2538-2550 (1999).
52. Thacker, D., Mohibullah, N., Zhu, X. & Keeney, S. Homologue engagement controls meiotic DNA break number and distribution. *Nature* **510**, 241-246 (2014).
53. Kara, N., Krueger, F., Rugg-Gunn, P. & Houseley, J. Genome-wide analysis of DNA replication and DNA double-strand breaks using TrAEL-seq. *PLoS Biology* **19**(2021).
54. Bishop, D.K., Park, D., Xu, L. & Kleckner, N. *DMC1*: A meiosis-specific yeast homolog of E. coli *recA* required for recombination, synaptonemal complex formation, and cell cycle progression. *Cell* **69**, 439-456 (1992).
55. Vader, G. *et al.* Protection of repetitive DNA borders from self-induced meiotic instability. *Nature* **477**, 115-121 (2011).
56. Fourel, G., Revardel, E., Koering, C.E. & Gilson, É. Cohabitation of insulators and silencing elements in yeast subtelomeric regions. *EMBO Journal* **18**, 2522-2537 (1999).
57. Radman-Livaja, M. *et al.* Dynamics of Sir3 spreading in budding yeast: Secondary recruitment sites and euchromatic localization. *EMBO Journal* **30**, 1012-1026 (2011).

bioRxiv preprint doi: https://doi.org/10.1101/2025.02.27.640173; this version posted March 3, 2025. The copyright holder for this preprint (which was not certified by peer review) is the author/funder, who has granted bioRxiv a license to display the preprint in perpetuity. It is made available under aCC-BY-NC-ND 4.0 International license.

58. Fourel, G. *et al.* An activation-independent role of transcription factors in insulator function. in *EMBO reports* Vol. 2 124-132 (2001).
59. Saxton, D.S. & Rine, J. Nucleosome Positioning Regulates the Establishment, Stability, and Inheritance of Heterochromatin in *Saccharomyces cerevisiae*. *PNAS* **117**, 27493-27501 (2004).
60. Ichikawa, Y., Morohashi, N., Nishimura, Y., Kurumizaka, H. & Shimizu, M. Telomeric repeats act as nucleosome-disfavouring sequences in vivo. *Nucleic Acids Research* **42**, 1541-1552 (2014).
61. Markowitz, T.E. *et al.* Reduced dosage of the chromosome axis factor Red1 selectively disrupts the meiotic recombination checkpoint in *Saccharomyces cerevisiae*. *PLoS Genetics* **13**(2017).
62. Su, Y., Barton, A.B. & Kaback, D.B. Decreased meiotic reciprocal recombination in subtelomeric regions in *Saccharomyces cerevisiae*. *Chromosoma* **109**, 467-475 (2000).
63. Lamb, N.E., Yu, K., Shaffer, J., Feingold, E. & Sherman, S.L. Association between maternal age and meiotic recombination for trisomy 21. *American Journal of Human Genetics* **76**, 91-99 (2005).
64. Sherman, S.L., Freeman, S.B., Allen, E.G. & Lamb, N.E. Risk factors for nondisjunction of trisomy 21. *Cytogenetic and Genome Research* **111**, 273-280 (2005).
65. Humphryes, N. & Hochwagen, A. A non-sister act: Recombination template choice during meiosis. *Experimental Cell Research* **329**, 53-60 (2014).
66. Medhi, D., Goldman, A.S. & Lichten, M. Local chromosome context is a major determinant of crossover pathway biochemistry during budding yeast meiosis. (2016).
67. Scherthan, H. A bouquet makes ends meet. *Nature Reviews Molecular Cell Biology* **2**, 621-627 (2001).
68. Blitzblau, H.G. & Hochwagen, A. ATR/Mec1 prevents lethal meiotic recombination initiation on partially replicated chromosomes in budding yeast. *eLife* **2**, 1-20 (2013).
69. Langmead, B. & Salzberg, S.L. Fast gapped-read alignment with Bowtie 2. *Nature Methods* **9**, 357-359 (2012).
70. Kar, F.M., Vogel, C. & Hochwagen, A. Meiotic DNA breaks activate a streamlined phospho-signaling response that largely avoids protein-level changes. *Life Science Alliance* **5**, 1-15 (2022).
71. Ewels, P.A.P.A.F.S. & et al. The nf-core framework for community-curated bioinformatics pipelines. *Nature Biotechnology* **38**, 271-271 (2020).
72. Patel H, E.P.P.A.H.n.R.B.O.S.G.M.D.V.P.M.S.L. & et al. nf-core/rnaseq: Nf-core/ rnaseq v3.1 - Lead Alligator (3.1). (2021).
73. Patro, R., Duggal, G., Love, M.I., Irizarry, R.A. & Kingsford, C. Salmon provides fast and bias-aware quantification of transcript expression. *Nature Methods* **14**, 417-419 (2017).
74. Heldrich, J., Sun, X., Vale-Silva, L.A., Markowitz, T.E. & Hochwagen, A. Topoisomerases Modulate the Timing of Meiotic DNA Breakage and Chromosome Morphogenesis in *Saccharomyces cerevisiae*. *Genetics* **215**, 59-73 (2020).